EXTRACTION OF BUILDING DAMAGE IN THE KUMAMOTO EARTHQUAKE FROM MULTI-TEMPORAL LIDAR AND PALSAR-2 DATA

Fumio Yamazaki[1], Luis Moya[2], and Wen Liu[1],

[1]Department of Urban Environment Systems, Chiba University, Japan; fumio.yamazaki@faculty.chiba-u.jp
[2]International Research Institute of Disaster Science, Tohoku University, Japan

ABSTRACT: Extraction of collapsed buildings from a pair of Lidar data and ALOS-2 PALSAR-2 data taken before and after the 2016 Kumamoto earthquake was conducted. Lidar surveys were carried out for the affected areas along the causative faults on April 15 and April 23, 2016. The spatial correlation coefficient of the two Lidar data was calculated and the horizontal shift of the April-23 digital surface model (DSM) with the maximum correlation coefficient was considered as the crustal movement by the April-16 main-shock. The both horizontal and vertical coseismic displacements were removed to extract collapsed buildings. The average of difference between the pre- and post-event DSMs within a building footprint was selected as a parameter to evaluate the collapse of buildings. The extracted height difference was compared with the spatial coherence value calculated from pre- and post-event PALSAR-2 data. Based on this comparison, the collapsed buildings could be extracted well by setting a proper threshold value for the average height difference.

KEY WORDS: Lidar, the 2016 Kumamoto earthquake, building damage, DSM, PALSAR-2

1. INTRODUCTION

Information gathering after a large-scale natural disaster is very important in emergency response and recovery activities. But the access to the affected areas is often hindered by the disruption of road networks. Thus remote sensing technologies have been employed to assess the extent and degree of various damages. Various high-resolution optical and SAR satellites have been in operation in the last decade and they were employed to observe affected areas after major natural disasters..

Various aerial surveying technologies have also been developed in the last few decades, such as digital aerial cameras, Lidar (Light detection and ranging), and more recently, unmanned aerial vehicles (UAVs, drones). Lidar is the most costly but the most accurate method to acquire digital surface models (DSMs), and hence it has been used to develop digital elevation models (DEMs) and 3D configuration of buildings (Vu et al., 2009). But applications of Lidar for damage detection are still few because the lack of Lidar data obtained before a disaster.

A series of earthquakes with Mw7.0 as the main-shock hit Kumamoto prefecture in Kyushu Island, Japan in April 2016. Among the several remote sensing technologies used to monitor the area affected by the Kumamoto earthquake, a pair of Lidar datasets taken before and after the main-shock were available (Asia Air Survey Co., 2016; Moya et al., 2017). This study explores the potential use of Lidar data to extract collapsed buildings over a wide area. The average of difference between the pre- and post-event DSMs within a building footprint was introduced to evaluate whether a building is collapsed or not. The result was compared with the spatial coherence value calculated from pre- and post-event ALOS-2 PALSAR-2 data.

2. THE 2016 KUMAMOTO EARTHQUAKE SEQUENCE

A Mw6.2 earthquake hit the Kumamoto Prefecture in Kyushu Island, Japan on April 14, 2016 at 21:26 (JST). A considerable amount of structural damages and human casualties had been reported due to this event, including 9 deaths. The epicenter was located in the Hinagu fault with a shallow depth. On April 16, 2016 at 01:25 (JST), about 28 hours after the first event, another earthquake of Mw7.0 occurred in the Futagawa fault, closely located with the Hinagu fault. Thus, the first event was called as the "foreshock" and the second one as the "main-shock". The epicenters of the both events were located in Mashiki Town, to the east of Kumamoto City.

Figure 1 shows the location of these causative faults and Japanese national GNSS Earth Observation Network System (GEONET) stations in the source area. The GEONET covers Japan's territory with about 1,300 stations. The displacement of 75 cm to the east-northeast (ENE) was observed at the Kumamoto station while that of 97 cm to the southwest (SE) at the Choyo station by the main-shock. These observations validated the right-lateral strike-slip mechanism of the Futagawa fault.

Extensive impacts due to strong shaking and landslides were associated by the Kumamoto earthquake sequence, such as collapse of buildings and bridges. A total of fifty (50) direct deaths were accounted by the earthquake sequence, mostly due to the collapse of wooden houses in Mashiki town and landslides in Minami-Aso village.
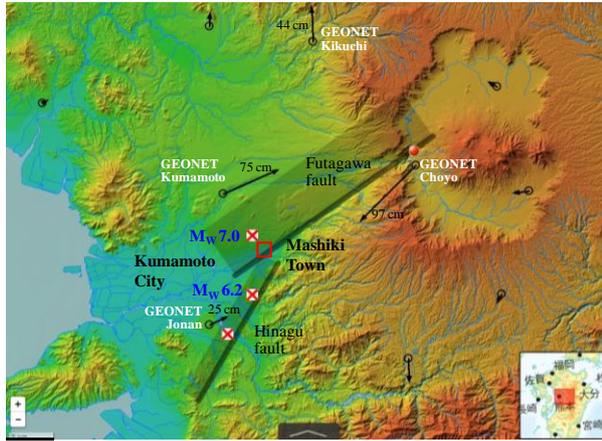
Figure 1. Location of causative faults and GNSS stations in the 2016 Kumamoto earthquake.

3. STUDY AREA AND DATASET

After the foreshock, a Lidar surveying flight was carried out during 15:00 – 17:00 (JST) on April 15, 2016, in order to record the effects of the earthquake (Asia Air Survey Co., 2016). It produced point clouds with an average point density of 1.5-2 points/m^2. Subsequently, because the unexpected main-shock occurred, a second mission was set up during 10:00 – 12:00 (JST) on April 23, 2016, which produced point clouds with an average point density of 3-4 points/m^2. The both sets of Lidar data were acquired using a Leica ALS50II instrument and the same pilot and airplane. After rasterization of the raw point clouds, two digital surface models (DSMs) with a data spacing of 50 cm were created.

The study area is located in the near field of the Kumamoto earthquake sequence where significant permanent ground displacements were produced. A direct comparison of the pre- and post-event DSMs shows that the building coordinates do not match because the post-DSM contains coseismic displacements. Thus, the post-DSM was shifted before detecting the damaged buildings based on the permanent crustal movement (Moya et al., 2017). **Figure 2** illustrates the calculated coseismic displacement for the common Lidar data area. The results of new field measurement carried out in August 2016 for surveying reference points after the Kumamoto Earthquake are also shown (GSI, 2016). The coseismic displacements estimated from the Lidar data show good agreement with the survey results.

4. EXTRACTION OF COLLAPSED BUILDINGS

To focus on buildings, a geocoded building footprint dataset, provided by the Geospatial Information Authority of Japan (GSI), was used. Only buildings with footprint areas greater than 20 m^2 were evaluated. Because the point densities of the two DSMs are different and the footprint data include some errors, perfect matching of the DSMs with the building footprints could not be
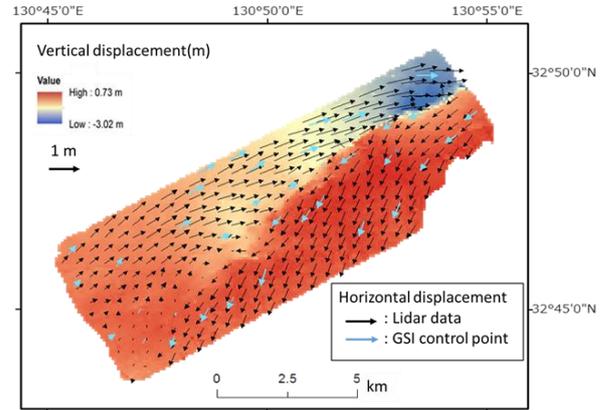

Figure 2. Estimated 3D coseismic displacement after the main-shock of the 2016 Kumamoto earthquake. The black arrows and shaded colors indicate the horizontal and vertical displacements obtained from the Lidar data by Moya et al. (2017). The blue arrows indicate the horizontal displacements at the control points measured by GSI (2016).
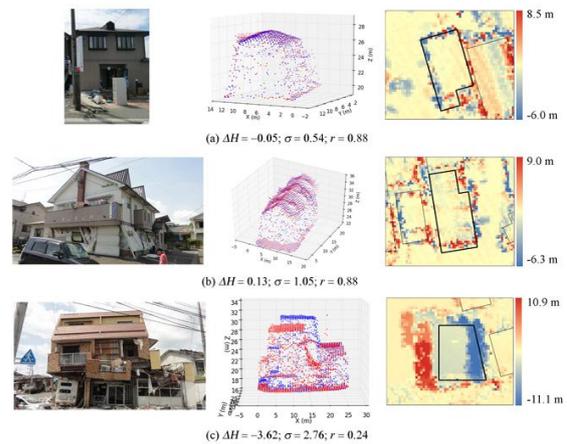

Figure 3. Examples of non-collapsed (a) and collapsed (b, c) buildings extracted using the Lidar data. The left figure shows the photos taken after the main-shock by the authors, the middle figure the two DSMs, and the right figure the elevation differences between the two DSMs..

achieved. Thus the building footprints were reduced by 1 m. The LiDAR data within the reduced building footprints were then extracted and processed. The reason for using the reduced footprints was to discard the DSM data near the footprints in the subsequent analysis.

Figure 3 shows three buildings in the study area. For each case, the pre-DSM (blue dots), the post-DSM (red dots), and the difference of the two DSMs are depicted. These buildings were selected in order to demonstrate different damage patterns: non-damaged, tilted, and collapsed buildings. The difference between the DSMs for a non-collapsed building (a) shows high values around the boundary of the building footprint. These errors are certainly present for tilted buildings as well (b).

Figure 3c shows a typical mid-story collapsed steel-frame building, in which the two DSMs and their difference highlight the damage pattern.

Figure 4 shows the relative vertical displacement calculated from the two Lidar DSMs, where blue colored pixels show the decrease of height, mostly due to the collapse of buildings. **Figure 5** shows the relationship between the height difference and the extracted area exceeding the plus and minus threshold value. For example, if 0.5-m is selected as the height difference threshold, about 8.5 % of the target area was extracted.

Although the Lidar DSMs have elevation accuracy of less than 10 cm, the location accuracy of laser cloud points is an order of 50 – 70 cm. Considering this situation, +0.5 m was determined as the height difference threshold of changes for the 0.5-m square grid Lidar data. It is recognized from the figure that the area of reduced-height pixels is about 1.6 times of the area of increased-height pixels. This observation can be explained by the fact that the reduced-height in this urban area was mostly due to the collapse of buildings and the increased-height was due to the accumulation of debris and the displacement of collapsed buildings to surrounding areas.
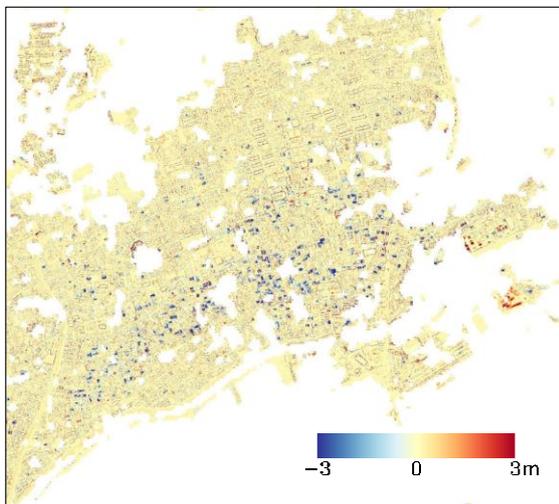

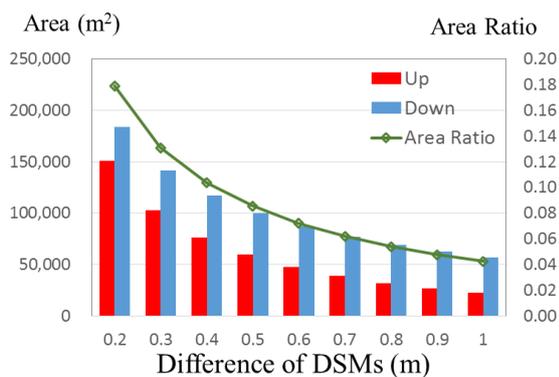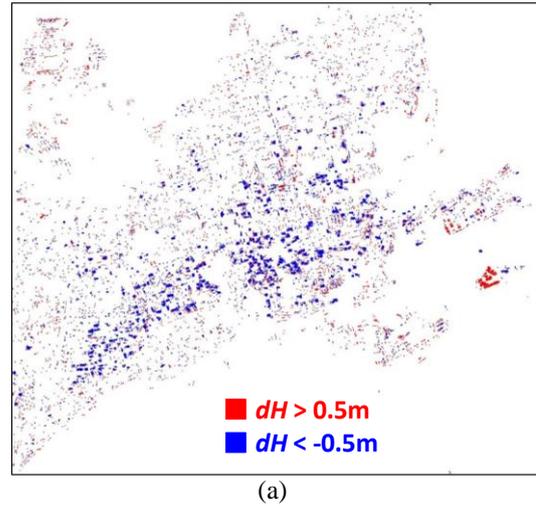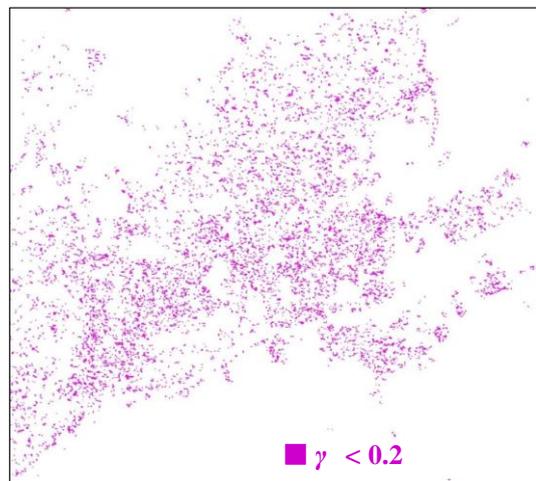**Figure 4.** The height difference of the two DSMs in the center of Mashiki Town.

Figure 5. Relationship between the height difference and the area exceeding the plus and minus thresholds.

Figure 6. Changed areas extracted by height-difference (abs. (dH) > 0.5 m) of the two DSMs (a); and changed areas extracted by low coherence (γ < 0.2) from PALSAR-2 data (b).

Figure 6 compares the possible changed areas extracted by height-difference (dH > 0.5 m or dH < -0.5 m) and those by low coherence (γ < 0.2) from pre- and post-event ALOS-2 PALSAR-2 data (Liu and Yamazaki, 2017). The PALSAR data were acquired on April 15 and 29, 2016, from a decending path No. 28 with left look. The range resolution is 1.43 m and the azimath resolution 1.74 m. In these extractions, the objects smaller than 9.0 m^2 were removed as noises, such as cars and debris. The distributions of the extracted areas were not the same but very similar although the situations of change for the two data sets have some different aspects.

The extracted areas from the Lidar DSMs were closely examined for the central part of Mashiki Town including the town office building as shown in **Figure 7**. It is seen from the figure that by increasing the height-threshold, the selected areas are seen to decrease. Increased-height pixels are seen to be mostly parking cars and some debris while decreased-height pixels are collapsed buildings. From the comparisons, the most
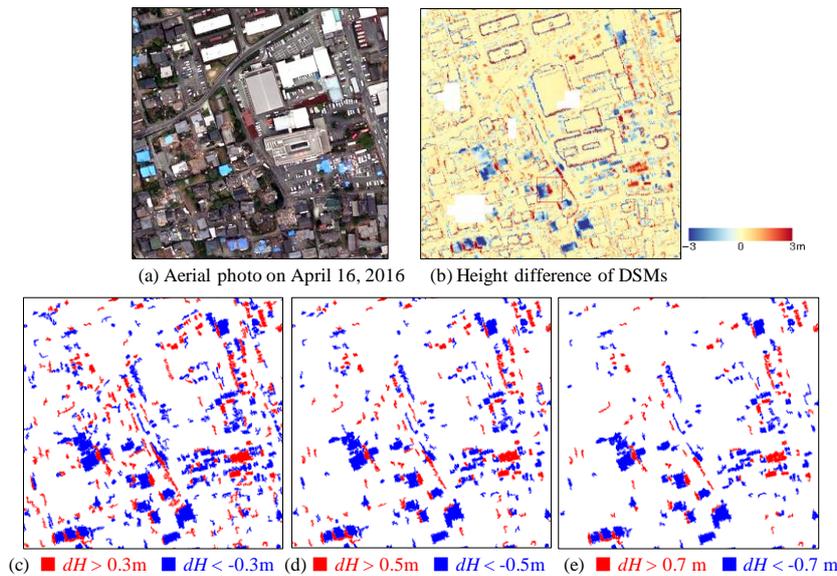
(a) Aerial photo on April 16, 2016	(b) Height difference of DSMs

(c) ■ *dH > 0.3m* ■ *dH < -0.3m*   (d) ■ *dH > 0.5m* ■ *dH < -0.5m*   (e) ■ *dH > 0.7 m* ■ *dH < -0.7 m*

Figure 7. Aerial photograph around Mashiki Town office (a), height difference of the two DSMs (b), and extracted areas by different height-difference values (c-e). Objects smaller than 9.0 m^2 were excluded.

suitable threshold value of the average height reduction within a reduced building footprint was determined as 0.5 m (Moya et al., 2018).

5. CONCLUSIONS

Extraction of collapsed buildings from a pair of Lidar data taken before and after the 2016 Kumamoto, Japan, earthquake was attempted. The spatial correlation coefficient of the two Lidar data was calculated and the horizontal shift of the April-23 digital surface model (DSM) with the maximum correlation coefficient was considered as the crustal movement by the April-16 main-shock. The horizontal component of the calculated coseismic displacement was applied to the post-event DSM to cancel it, and then the vertical displacement between the two DSMs was calculated. After removal of the horizontal and vertical coseismic displacements, building-footprints were employed to assess the changes of the DSMs. The average of differences between the pre- and post-event DSMs within a building footprint was selected as a parameter to evaluate the collapse of buildings. The extracted height difference values were compared with the spatial coherence values calculated from pre- and post-event ALOS-2 PALSAR-2 data. The comparison result indicates that the collapsed building can be extracted by setting a proper threshold value, plus and minus 0.5 m within a building footprint, and the selected total areas were closed to low coherence ($\gamma < 0.2$) areas from the pre- and post-event PALSAR-2 data.

References

Asia Air Survey Co., Ltd., 2016. The 2016 Kumamoto earthquake, http://www.ajiko.co.jp/article/detail/ID5725U VGCD/ (accessed on 4 March 2018).

Geospatial Information Authority of Japan (GSI), 2016. the 2016 Kumamoto Earthquake (in Japanese), http://www.gsi.go.jp/BOUSAI/H27-kumamoto-earthquake-index.html (accessed on 4 March2018).

Liu, W. and Yamazaki, F., 2017. Extraction of collapsed buildings due to the 2016 Kumamoto earthquake based on multi-temporal PALSAR-2 data, *Journal of Disaster Research*, 12(2), pp. 241-250.

Moya, L., Yamazaki, F., Liu, W., Chiba, T., 2017. Calculation of coseismic displacement from lidar data in the 2016 Kumamoto, Japan, earthquake, *Natural Hazards and Earth System Sciences*, 17, pp. 143-156.

Moya, L., Yamazaki, F., Liu, W., Yamada, M., 2018. Detection of collapsed buildings due to the 2016 Kumamoto, Japan, earthquake from Lidar data, *Natural Hazards and Earth System Sciences*, 18, pp. 65-78

Vu, T.T., Yamazaki, F. and Matsuoka, M., 2009. Multi-scale solution for building extraction from LiDAR and image data, *International Journal of Applied Earth Observation and Geoinformation*, 11, pp. 281–289.